



Assessment of Grinding Burn of AISI D2 Tool Steel Using Barkhausen Noise Technique

Atul Kumar Shrivastava¹ · Ashwani Sharma¹ · Akash Subhash Awale¹ · Mohd Zaheer Khan Yusufzai¹ · Meghanshu Vashista¹

Received: 19 December 2020 / Accepted: 3 June 2021 / Published online: 16 June 2021
© The Institution of Engineers (India) 2021

Abstract The aim of present study is to experimentally investigate and compare the effect of grinding parameters, i.e. downfeed, work velocity and lubricating environments, on the surface integrity of hardened AISI D2 tool steel. The surface integrity of ground surface was evaluated in terms of surface roughness, surface topography, microstructure and microhardness variation. Grinding performance was investigated concerning grinding force, specific grinding energy and grinding temperature. Quasi-steady-state moving heat source model was used to estimate grinding temperature under different environments, viz. dry and flood. The second objective of the present work is the non-destructive evaluation of thermally damaged ground surface by the novel Barkhausen noise technique. The results showed that flood environment reduces grinding force, specific grinding energy and grinding temperature owing to effective cooling and lubrication medium. A thick redeposition layer over ground surface along with minimum surface roughness was observed under dry grinding. Further, drastic change in microstructure and microhardness was observed under dry environment due to a number of passes of grinding wheel over ground surface without coolant, which induced excess heat and developed martensite layer near the nascent surface. Finally, poor BN response such as lower root mean square (rms) and peak value was found in thermally damaged sample owing to large obstacles for magnetic domain wall displacement.

Keywords AISI D2 tool steel · Grinding temperature · Surface topography · Microhardness · Microstructure · Barkhausen noise

Introduction

A large section of engineering components need high-dimensional accuracy and excellent surface finish, which is usually challenging to achieve by conventional machining like turning and milling. Besides, manufacturing sectors face problems while machining “difficult-to-cut” materials like Inconel, titanium, tool steel, hardened steels [1, 2]. In such cases, grinding is an effective tool to enhance the surface integrity of “difficult-to-cut” materials. However, grinding is complex phenomena because of randomly oriented multi-point cutting grains, which cut the work material with high-velocity abrasive wheel [3]. Hence, a huge amount of conventional cutting fluid was utilized in grinding to maintain the surface integrity of ground samples. Conventional cutting fluid is petroleum-based cutting fluid, which produces a negative impact on machine operator’s health and environment [4]. Manufacturing industries have been compelled to consider dry grinding to enforce environmental protection laws for occupational safety and health regulations. Moreover, dry machining shows positive effects such as thermal shock reduction and minimum comb crack formation in the components [5].

The physical surface condition of a ground component is expressed in surface integrity, which includes knowledge about surface topography, microhardness and microstructure aspect of the machined surface [6]. Apart from this, surface integrity significantly affects the product working life as pitiable surface integrity may cause the breakdown of a component before their predicted working life. Hence,

✉ Meghanshu Vashista
mvashista.mec@iitbhu.ac.in

¹ Department of Mechanical Engineering, Indian Institute of Technology (BHU), Varanasi 221005, India

several manufacturing industries were adopted conventional testing techniques for surface integrity characterization such as microhardness measurement, optical microscope and X-ray diffraction. All these techniques provided accurate results, but these are costly, time-consuming, destructive and laboratory-based methods [7]. Barkhausen noise (BN) technique is an effective substitute for conventional testing methods because it provides fast and reliable outcomes and is also used in in-line production. The measurement using Barkhausen noise is based on the fact that physical and mechanical properties alter the magnetic domain structure of ferromagnetic materials. The generation of BN signal is due to discrete changes in the magnetization of ferromagnetic material, when it is kept under an external field. The defects in microstructure in the form of impurities, grain boundaries, phase transformation and residual stress act as the strong barrier and thus hinder the domain wall motion, which affects the BN signal [8].

Many research groups experimental studied the effect of grinding environments on the surface integrity of various engineering materials using non-destructive Barkhausen noise techniques. For example, Moia et al. [9] monitored the alumina grinding wheel during dressing operation using acoustic emission (AE) signal and artificial neural networks. A single-point dresser was used in the grinding experiment. They found sharp cutting edges with improvement in cutting capacity of alumina wheel at optimal dressing conditions. Hadad and Sharbati [10] performed the test in dry, flood, MQL with compressed air, MQL with argon condition. The experimental outcomes indicated that dressing speed significantly influence the grinding performance as followed by dressing depth. Manimaran et al. [11] performed grinding experiments on AISI 316 stainless steel with an alumina wheel under dry, wet and cryogenic conditions. They found a reduction in grinding forces, temperature and surface roughness at higher work speed and liquid nitrogen pressure under cryogenic condition. Tawakoli et al. [12] reported that the impact of the different types of abrasive wheel, i.e. CBN and Al_2O_3 (low and high porosity, coarse grain type), on hardened 100Cr6 steel under minimum quantity lubrication (MQL) grinding. They found that better surface quality and less grinding forces with CBN wheel and also obtained reasonable grinding outcomes due to the coarser and high-porosity Al_2O_3 wheel. Nahak et al. [13] reported that rms and peak value decreases with an increase in microhardness of electrical discharge machined high-carbon high-chromium (HCHCr) die steel using nondestructive Barkhausen noise technique. Jiles [14] discussed the effect of grain size on the BN signal. As the grain size becomes smaller, the number of pinning sites increases. This results in higher Barkhausen jumps but smaller amplitude. Srivastava et al. [15] also observed a decrease in BN (rms)

with an increase in microhardness of material owing to hamper in the motion of domain wall of hardened IS 2062 steel upon dry grinding.

The aim of the present work is an experimental investigation of the grindability of AISI D2 tool steel under different environments. Quality of ground surface was studied with special attention to surface integrity responses like surface roughness, surface topography, microstructure and microhardness. Finally, surface integrity response such as microhardness was correlated with BN outcomes like rms and peak. These BN signal were obtained at different magnetic field intensity and magnetizing frequency to a faster assessment of thermally damaged ground samples.

Experimental Procedure

Hardened AISI D2 tool steel was utilized as workpiece during grinding ($100 \times 20 \times 8$ mm), which is well known for its high wear and corrosion resistance and high compressive strength. Hence, AISI D2 tool steel was widely used in tooling industries for producing punch, stamping and injection dies. The sample was heat-treated to achieve the acceptable hardness of tooling components. The hardness of the work material varies in the range of 55 ± 2 HRC. In the heat treatment process, each sample was heated gradually up to 650°C , held to the temperature up to uniform heating of all surface and continues heating until 1050°C for 90 min in the vacuum furnace. Then, samples cooled in an oil quench. These samples were primarily tempered at 400°C for 120 min and secondarily tempered at 450°C for 120 min for improvement in toughness and relief of internal stresses due to quenching. The optical images of unhardened and hardened AISI D2 tool steel are illustrated in Fig. 1. The experiment was performed on work material using H455 HMT surface grinding machine with WA-46-K-5-V8 alumina wheel. Typically, Al_2O_3 wheel was utilized for a wide range of carbon steels because of no chemical affinity between both materials, further self-resharpening of alumina grits during grinding of ferrous material; as a result, minimum forces act on the grits during shearing action of work material [16]. Researchers reported that the grinding depth of cut and table feed significantly affected grindability indices and surface integrity of “difficult-to-cut” materials like Ti-6Al-4 V alloy [17], hardened AISI H13 die steel [18] and stainless steel [19]. Hence, a number of trial experiments were performed on the workpiece to find the optimum grinding parameters. Based on Taguchi L18 orthogonal array, a final experiment was designed. The experimental conditions are illustrated in Table 1.

A 3D dynamometer was used for tangential and normal grinding force measurement (Model-610C, IEICOS) with a

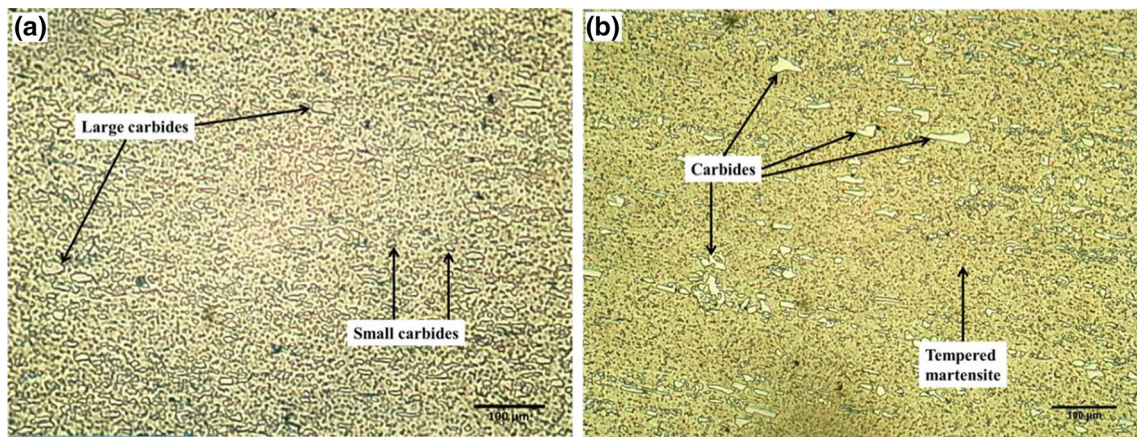


Fig. 1 Optical photographs of AISI D2 tool steel: **a** received sample, **b** heat-treated sample

Table 1 Experimental and characterization conditions

Grinding conditions	Value
Grinding mode	Plunge grinding
Grinding wheel	Al ₂ O ₃ wheel
Work material	AISI D2 tool steel
Wheel velocity (V_s)	39.46 m/s
Downfeed (a_p)	8, 16, 24 µm
Work velocity (V_w)	8, 10, 12 m/min
Environmental conditions	Flood and dry
Dresser	Single-point diamond
Dressing depth	20 µm × 15 times
Dressing speed	2800 rpm
Number of BN cycles	3
BN gain	20 db
BN filter range	10–300 kHz
BN magnetizing frequency (MF) at constant MFI: 1000 Oe	10, 20, 30, 40 Hz
Magnetic field intensity (MFI) at constant MF: 25 Hz	300, 600, 900, 1200 Oe

sampling rate of 1000 Hz, frequency filter range of 0–45 kHz and resolution of 0.1 kgf. The average grinding force (15 passes) was taken under each test condition. A high-precision stylus-based Mitutoyo SV-2100 surface roughness tester was utilized to trace the surface profile in the transverse direction of grinding. Surface roughness was measured at three different locations of each ground sample. The details of roughness measurement are as follows: traverse speed of 0.02 mm/s, cut-off length of 0.8 mm and transverse length of 4.0 mm. Moving heat source model was used to determine the grinding temperature of the nascent ground surface. Further, to study the effect of thermal damage on the surface integrity of ground surface under dry and flood modes; four ground samples were selected on the basis of high and low grinding temperature

and visual inspection of the samples. Hence, these samples were cut to the grinding direction with the help of a precision abrasive cutting machine. The abrasive cutting machine specification as follows: cutting speed of 3500 rpm, abrasive cutter diameter of 285 mm and 1 mm thickness of the abrasive cutter. Table 2 list the sample selection criteria based on thermal damage for BN analysis.

These four samples were consecutively cold moulded and polished on the different mesh size of emery papers like 240, 320, 600, 800, 1000 and 1200 grades using polishing machine. Optical microscopic (make Dewinter) was utilized for observation of microstructure of the ground surface. Vickers microhardness tester (model MMV-SA, Micro Mech Technologies, India) was used to find the microhardness variation in the ground surface at 200 gm applied load for 15 s dwell time. The microhardness measurement was performed along the cross section of the ground sample up to 200 µm depth from ground surface with 20 µm regular intervals at 3 different locations of each sample. The BN test of thermally damaged samples was done with the help of MAGSTAR system (Technofour, India). In BN technique, magnetic field intensity (MFI) and magnetizing frequency (MF) are essential BN process parameters to find out the thermal damage effect through a magnetic domain wall movement against the magnetic field. These parameters depends on physical properties of the work material, such as residual stresses [20], volume fraction of ferrite–pearlite and martensite phases [21] and hardness variation [22]. In the present work, the ground sample was analysed in a wide range of MFI and MF. But, after MFI 1200 Oe and MF 40 Hz, no significant variation in BN responses was found. Hence, thermal damage of ground surface was evaluated in the range of MFI: 300–1200 Oe and MF: 10–40 Hz, respectively. Figure 2a, b shows grinding experimental arrangement and Barkhausen noise instrument for the assessment of ground samples.

Table 2 Selected sample for BN analysis

Downfeed (μm)	Work velocity (m/min)	Grinding environment	Grinding zone temperature ($^{\circ}\text{C}$)	Symbol
8	12	Flood	214	F1
16	10	Flood	446	F2
16	10	Dry	542	D1
24	8	Dry	1221	D2

Results and Discussion

Grinding Force

Figure 3 shows the variation of tangential and normal grinding force with different work velocity and downfeed. The tangential grinding force shows a variation from 16 to 66 N under flood mode and 22 N to 97 N under dry environment. Similarly, normal grinding force shows a variation from 41 to 160 N under flood mode and 54 N to 244 N under dry environment. This wide variation range indicated that the sliding and ploughing action were dominated over shearing action during microchip formation. This variation may be attributed to the combined result of maximum grit depth of cut (h_m) and shearing action. Maximum grit depth of cut increases with an increase in downfeed and resulted in an increase in the penetration of grit into ground surface; thus, grinding forces increase. Besides, h_m also increases with an increase in work velocity. But, in this case, sliding and ploughing action dominate over the increased h_m effect [23]. When work velocity decreases, it results in an increase in the number of abrasive grits interacting with the work surface for a longer periodic time. In other words, it increases the area of interaction of a single grit; as a result, more sliding and ploughing action dominates, which further increases the grinding forces. These results agreed with Thiagarajan et al. [24] when investigated the effect of cylindrical grinding parameters on grinding force and surface roughness of Al/SiC MMC. They reported that tangential force increases with a decrease in work velocity owing to wheelwork interfaces for a longer duration. Flood grinding was yielded the lowest tangential and normal grinding force (16 N and 41 N) as compared to dry environment due to sufficient cooling and lubrication medium. Furthermore, the coolant generated a strong lubricating film over ground surface, which decrease the coefficient of friction between ground surface and abrasive wheel, resulting in the decrease in the grinding force. Figure 3 also shows an abrupt increase in grinding forces with lowest work velocity under dry environment. It happens due to very slow work velocity and the absence of lubrication, which enhanced sliding action compared to shearing and

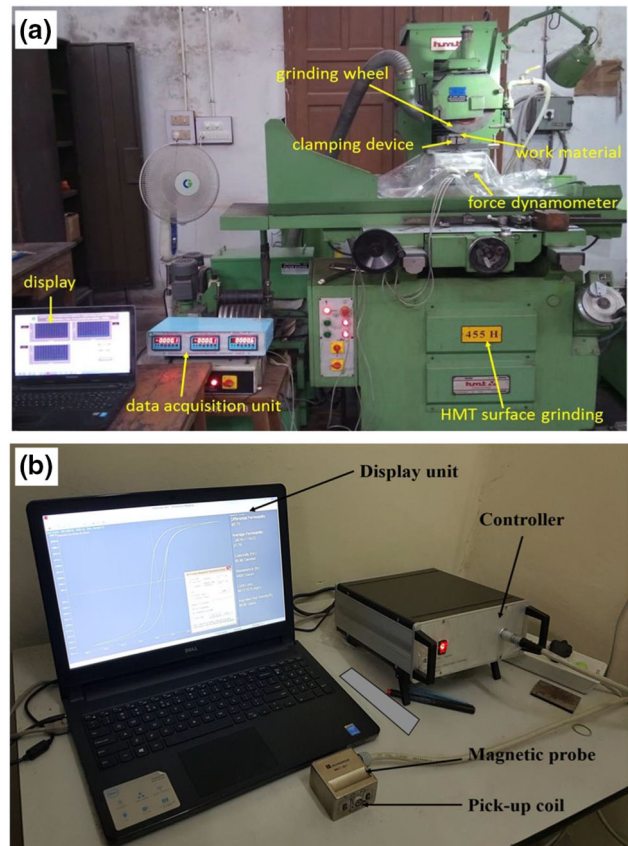


Fig. 2 a Grinding experimental set-up, b Barkhausen noise analyser for assessment of ground samples

ploughing action between abrasive grit and work surface, thus unexpectedly increasing the grinding force.

Specific Grinding Energy

Specific grinding energy (u_g) is known as the remove of material per unit volume from the work material. It is calculated by Eq. 1 [18].

$$u_g = \frac{60F_t V_s}{V_w a_p b} \quad (1)$$

where F_t is tangential force in N, V_s is grinding wheel speed in m/s, V_w is work velocity in m/min, a_p is downfeed

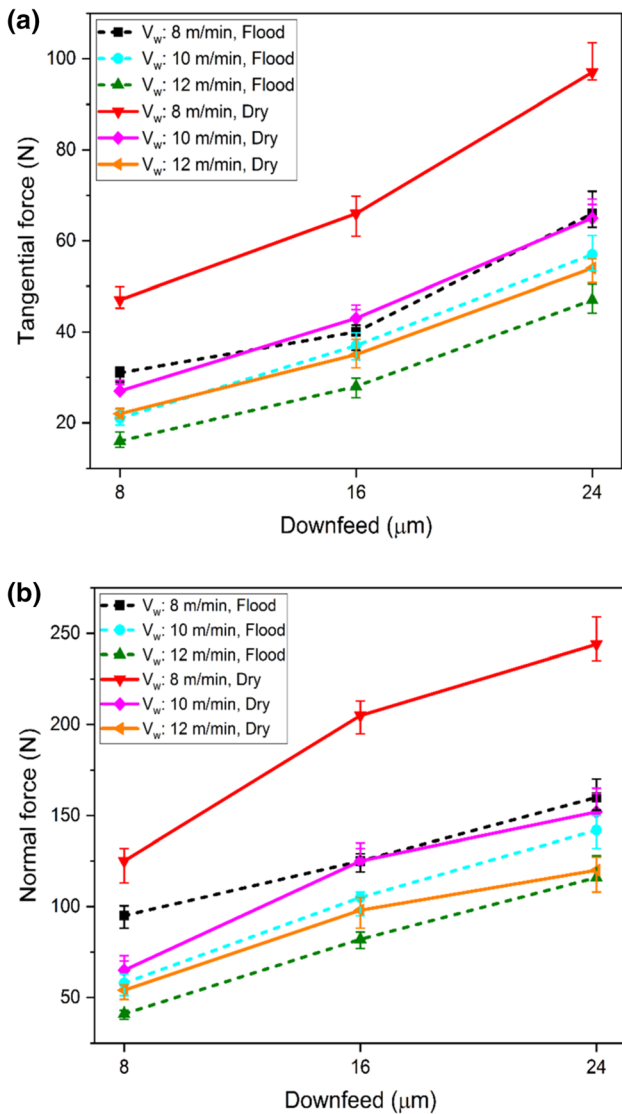


Fig. 3 Effect of different grinding environments on grinding force: **a** tangential force, **b** normal force

in \$\mu\text{m}\$ and \$b\$ is width of contact between grinding wheel and workpiece in mm.

High specific grinding energy describes the high power consumption and more contribution of ploughing and rubbing action of randomly oriented abrasive grits over the machined surface. Generally, more role of the shearing action as followed by ploughing and rubbing action indicates low specific grinding energy. Figure 4 reveals the variation in specific grinding energy with various work velocity and downfeed under dry and flood environments. At low downfeed, high grinding energy was observed in dry environment compared to flood environment. Further, specific grinding energy decreases with an increase in the downfeed in both respective environments. This happens due to more friction force between the grinding wheel and workpiece in the grinding zone. A high friction force

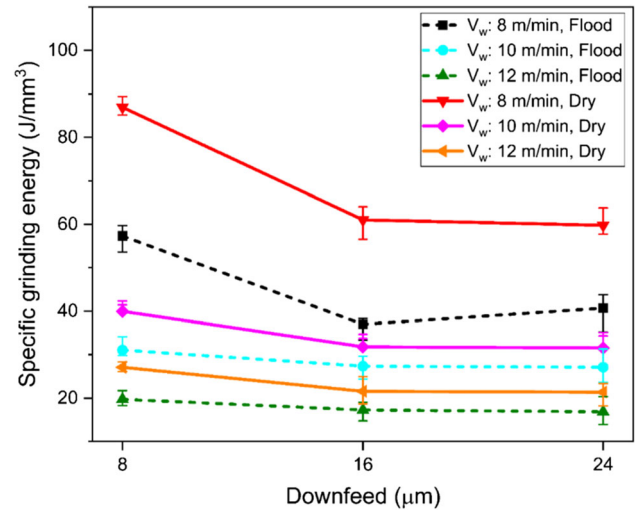


Fig. 4 Effect of different grinding environments on specific grinding energy

generates high specific energy. Lower specific grinding energy was obtained in flood grinding as followed by dry grinding because of lubrication at the contact area between the workpiece and grinding wheel. The specific grinding energy was 57.34, 36.99 and 40.69 J/mm³ at 8 m/min work velocity, respectively, which was 34.04, 39.40 and 46.98% lower than dry environments in the grinding process.

Estimated Grinding Temperature

Grinding temperature of the nascent ground surface was estimated using the quasi-steady-state moving heat source model proposed by Rowe [25]. The grinding temperature can be estimated by Eq. 2:

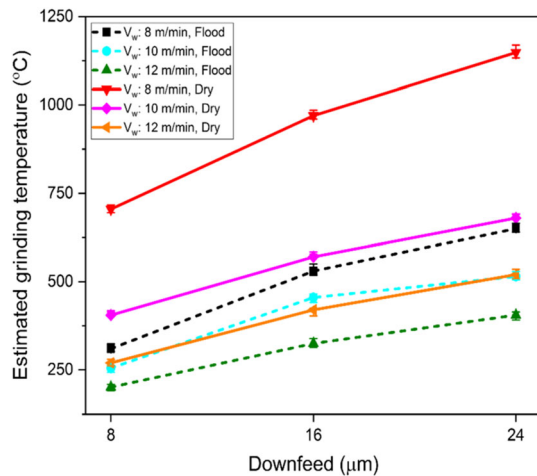
$$\theta = A \frac{\eta \times q_t}{\sqrt{k \times \rho \times c} \sqrt{V_w}} \sqrt{L_c} \tag{2}$$

where \$\theta\$ is grinding temperature, \$A\$ is a factor depending on downfeed, thermal properties of work material, \$q_t\$ is total heat flux in the contact length, \$k\$ is thermal conductivity of sample, \$c\$ is specific heat of sample, \$\rho\$ is density of sample, \$V_w\$ is the work velocity, \$\eta\$ is the apportionment coefficient, i.e. ratio of heat into workpiece and \$\eta = k / (k + k_g)\$, \$k_g\$ is the thermal conductivity of grinding wheel [26]. \$L_c\$ is contact length between grinding wheel and work material, which is calculated by \$L_c = a_p \times d_g\$. \$a_p\$ denoted as downfeed, and \$d_g\$ denoted the grinding wheel diameter. Similarly, Hadad et al. [27] also estimated grinding temperature during MQL grinding of hardened 100Cr6 steel using quasi-steady-state moving heat source model. The thermal properties of abrasive wheel and work material are illustrated in Table 3.

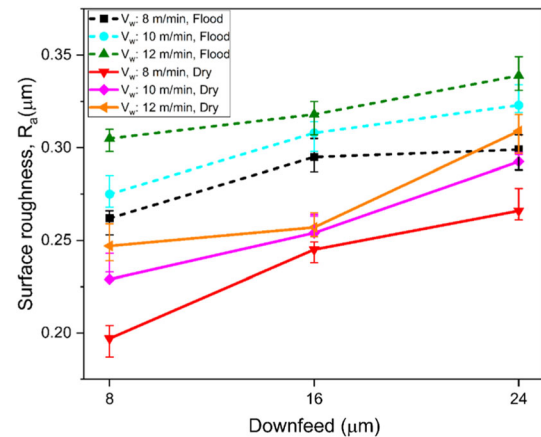
Figure 5 shows the effect of dry and flood environment on grinding temperature. The grinding temperature was

Table 3 Thermal properties of work material and grinding wheel

Elements	Density (kg/m ³)	Specific heat capacity (J/kg K)	Thermal conductivity (W/m K)	Thermal diffusivity (m ² /s)
AISI D2 tool steel	7,700	460	20.5	1.23×10^{-5}
Al ₂ O ₃ wheel	3,970	765	46	1.52×10^{-5}

**Fig. 5** Grinding temperature under different environments

found to vary from 214 to 658 °C in the case of flood environment, whereas temperature varies from 270 to 1158 °C in the dry environment. In flood grinding, 5–10% cutting oil was emulated in tap water and resulted in higher heat transferred from the grinding zone through water contents and uniform lubricating between wheelwork interfaces by cutting oil content [28]. The highest grinding temperature was observed under dry grinding due to the absence of cooling and lubricating media. This huge heat penetrates in ground surface and resulted in thermal damage to the work material. Further, this heat adversely affects surface integrity parameters, including an increase in microhardness and change in microstructure, i.e. phase transformation of ground surface and subsurface. Figure 5 also indicates that grinding temperature increases with an increase in the downfeed and decrease in the work velocity. This is due to abrasive grits that tend to plough instead of shearing at minimum work velocity and enhanced the intermittent effect between work and wheel contact. Similarly, Paknejad et al. [29] concluded that a long time was required to separate the abrasive wheel from ground surface at lower table feed, which induced high heat in the grinding zone and subsequently penetrated in the work material, i.e. X20Cr13 steel.

**Fig. 6** Effect of downfeed on surface roughness under different environments

Surface Roughness

Surface roughness depicts the surface quality of the finished parts. Roughness is a part of surface texture, which is utilized to find out the micro irregularities on the machined surface. The variation of centre line average roughness, i.e. R_a of ground surface, in the perpendicular direction of grinding under different environments is illustrated in Fig. 6. R_a was found to be dependent on the maximum grit depth of cut (h_m) and wheel loading condition. R_a was found to vary from 0.26 to 0.34 μm in the case of flood environment and from 0.19 to 0.31 μm in the dry environment. In all respective cases, R_a was found to be really low due to the high hardness of the work material, which restricts the shearing action of abrasive grits. Besides, average surface roughness was found to be less in the case of a dry environment as followed by flood environment. The high hardness of work material, high grinding force and absence of lubricating medium lead to very high temperature in grinding zone, which promotes welding of hot microscopic microchips to abrasive grit in dry grinding. Welding of grinding microchips to grits and inter-grit space in wheel makes the cutting edges of grits blunt and sliding, ploughing action dominates over shearing, which further increases plastic deformation of the nascent surface, resulted in a reduction in surface roughness under dry environment. Sinha et al. [30] also concluded that higher grinding temperature affects surface quality in large phase

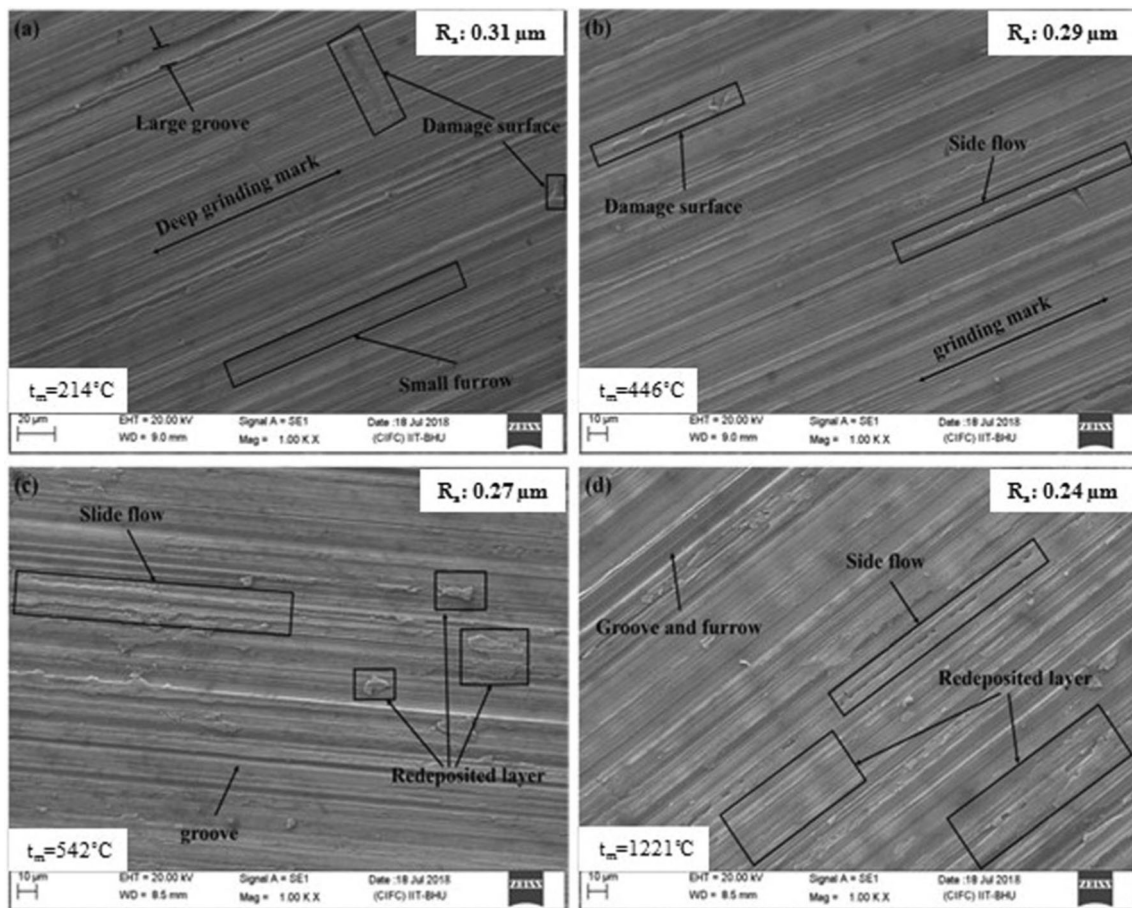


Fig. 7 Ground surface micrograph under different environments: **a** F1, **b** F2, **c** D1, **d** D2 samples

deformation and a decrease in surface roughness of ground Inconel 718 under dry grinding. R_a was found to increase with an increase in the downfeed and work speed, which can be attributed to increased chip volume or maximum grit depth of cut in both flood and dry environment.

Ground Surface Topography

Surface topography and surface roughness are two important terms, which determine the surface integrity of the finished component [31]. In the present study, surface roughness and 2D surface topography were investigated on the basis of highest and lowest thermal damage. Figure 7 indicates the SEM micrograph of ground surface under dry and flood conditions. In Fig. 7a, b, large groove and furrow, and deep grinding mark with maximum surface roughness (R_a 0.31 μm and R_a 0.29 μm) were observed under flood grinding due to a strong lubricating layer become develop over the nascent ground surface, which restricts the heat penetration in the sample, resulting in more shearing action on the work material through

grinding wheel as compared to sliding and ploughing action. Figure 7c clearly shows more side flows, and few furrows were observed on the ground surface under dry grinding due to the dominating effect of ploughing action over the shearing action. Further, large redeposited layers were observed over the ground surface (refer to Fig. 7d). These redeposited layers were developed due to the adhesion of microchips over ground surface at elevated temperature; microchips adhered in the pores of grinding wheel due to low thermal conductivity of work material. These microchips redeposited over ground surface in the next forward pass. The redeposition layer mechanism indicates transferring the atoms from one surface (microchip) to another surface (ground sample), with dominant carbon and oxygen elements. This observation agrees with Awale et al. [32], who observed a recast layer on ground AISI H13 die steel during dry grinding owing to high oxidation or carburization (C 16.56% and O 9.17%) of melted microchip over the ground surface. Paul et al. [33] also observed a thin redeposition layer along with plastic deformation of ground surface during dry grinding of Ti-

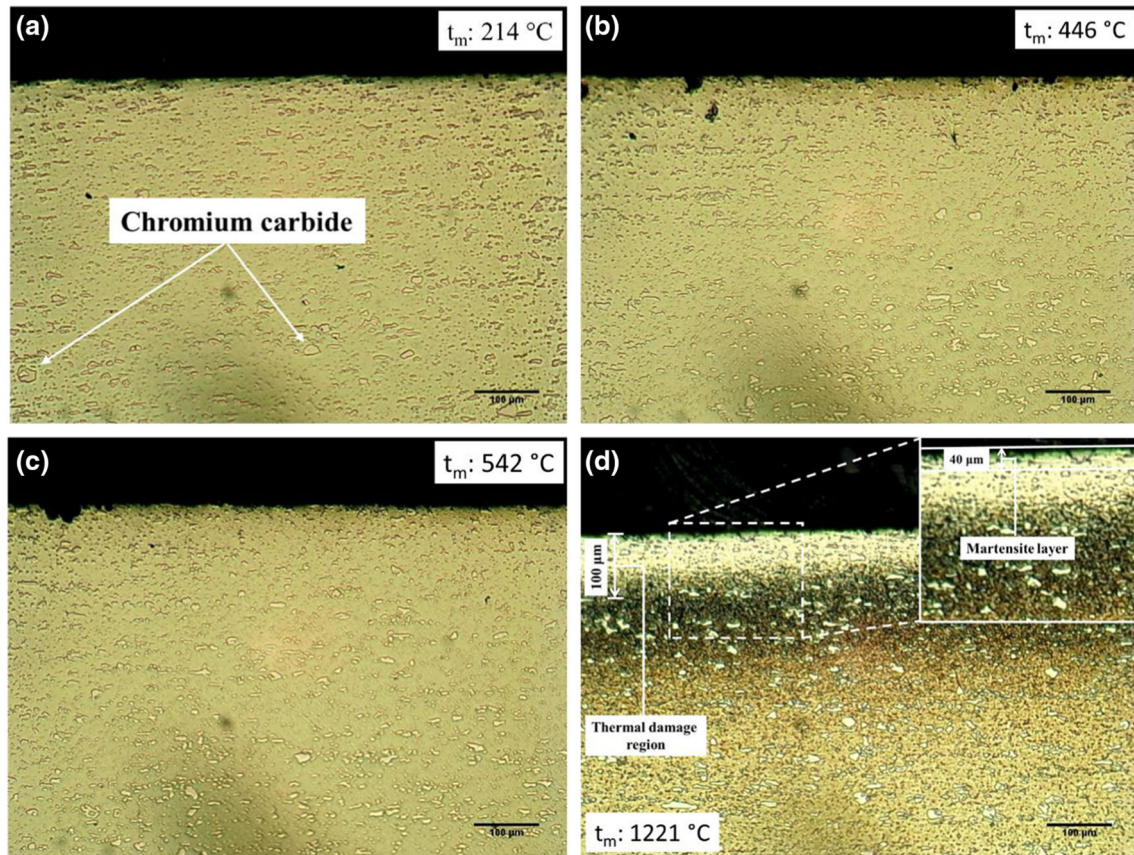


Fig. 8 Microstructural changes in ground sample under different grinding conditions: **a** F1, **b** F2, **c** D1, **d** D2 samples

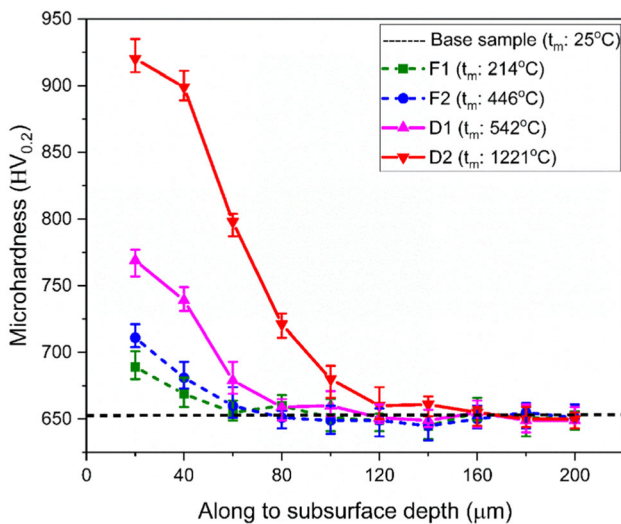


Fig. 9 Variation of microhardness along to subsurface depth under different environments

6Al-4 V. Further, the lowest surface roughness (R_x 0.24 μm) was obtained in the maximum thermal damage sample. This happens due to large plastic deformation of ground surface, which enhanced the sliding action of abrasive grits over the ground surface as compared to shearing and ploughing.

Microstructure and Microhardness

It is well known that excessive heat penetrates in the work material during grinding. This high temperature induced lattice distortion in the work matrix in the form of plastic deformation along the subsurface. Figure 8 shows the optical micrographs of the thermally damaged ground samples under different environments. Microstructure was observed along the cross section of ground surface for effective assessment of thermal damage. Figure 8a shows a typical microstructure of work material after flood grinding, i.e. F1 sample. It consists of uniformly dispersed chromium-rich alloy carbides in a matrix of tempered martensite. Carbides were formed in two different sizes in the matrix, some large carbides and rest smaller carbides. Precipitation hardening that means tempered martensite matrix and small chromium-rich carbides caused by maximum hardness of work material. According to Fig. 8b, c, it can be depicted that a very small variation in microstructure near ground surface due to grinding temperature developed below the austenitizing temperature of work material. Figure 8d clearly shows drastic microstructural change occurs in sample D2. Thus, D2 sample was exposed at 1221 °C during dry grinding. This localized heating with slower cooling due to the absence of coolant affected the

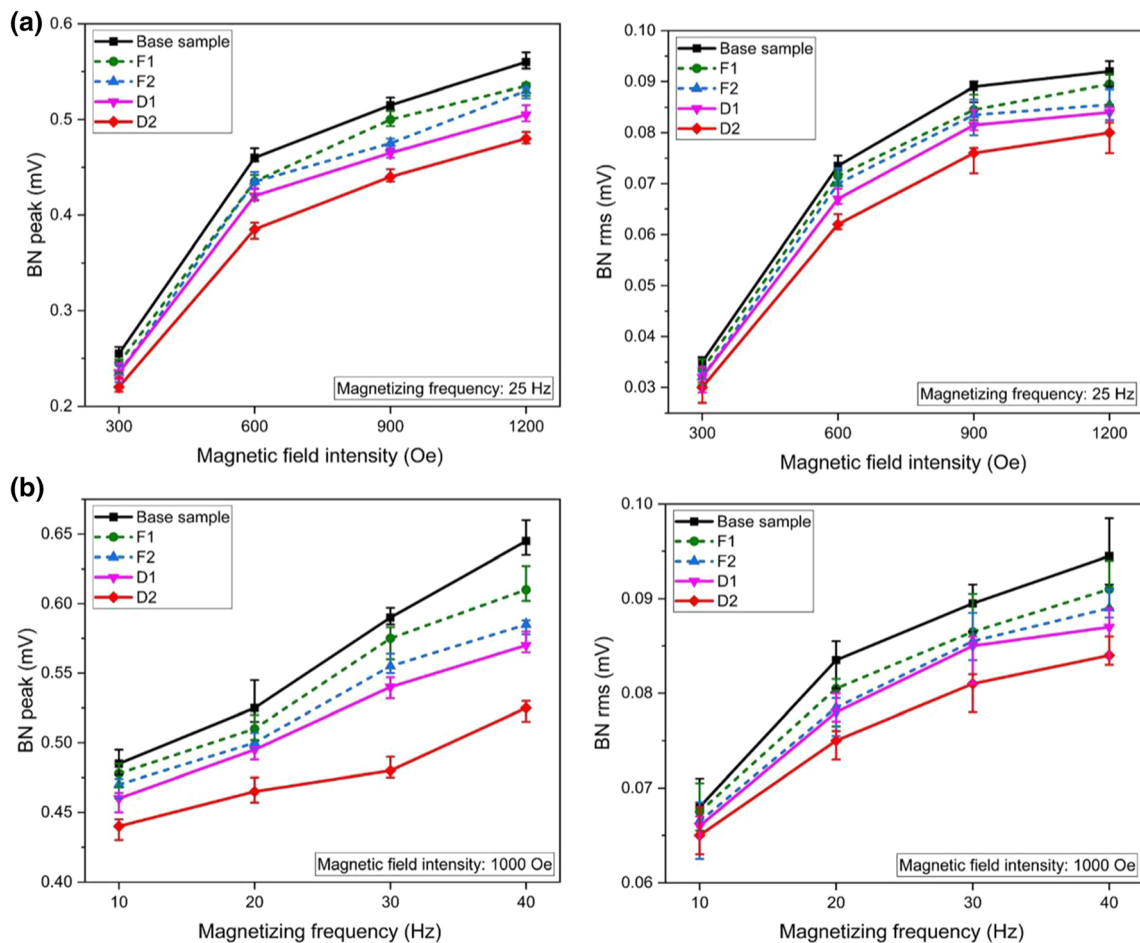


Fig. 10 Variation in BN responses under different grinding conditions: **a** magnetic field intensity, **b** magnetizing frequency

microstructure of ground sample in the form of grain refinement with fine carbides formation over entire nascent surfaces. Also, it can be noticed that maximum grinding temperature was observed during grinding of D2 sample, which was beyond the austenitizing temperature of work material. This resulted in the formation of a thin redeposited or rehardening layer (martensite layer) up to 40 μm depth in the subsurface of D2 sample. Further, overall thermal damaged surface (100 μm) was found in the case of dry grinding with higher downfeed. ImageJ software was utilized for measurement of the thermal damaged region of ground surface on the basis of microhardness indentation variation at a different location along the subsurface (refer to Fig. 9).

Figure 9 shows the microhardness profile of the ground sample along the subsurface under different environments. Four ground samples, i.e. F1, F2, D1 and D2, were selected for microhardness analysis on the basis of maximum thermal damage under dry and flood grinding. Lower microhardness (681 HV) was obtained in F1 sample,

whereas highest microhardness (943 HV) was obtained under lower work velocity (8 m/min) and higher downfeed (24 μm) in maximum thermally damaged ground sample. In D2 sample, high uniform hardness was observed in the subsurface up to 40 μm because of martensite layer formation. Further, hardness drastically decreased up to 100 μm depth owing to the work hardening effect of D2 sample as shown in Fig. 9. This occurred due to the penetration of maximum heat in the ground surface, which induced large scale plastic deformation and grain refinement near ground surface and subsurface. In the case of F1, F2, D1 sample, lower microhardness was obtained as compared to D2 sample. This may be attributed to faster heating and slower heat dissipation, which causes thermal softening of the nascent ground surface. Shaw [34] also found the minimum hardness of ground surface during grinding of hardened AISI 52,100 bearing steel because of high heat present in the workpiece for a long period of time. Furthermore, maximum temperature was developed

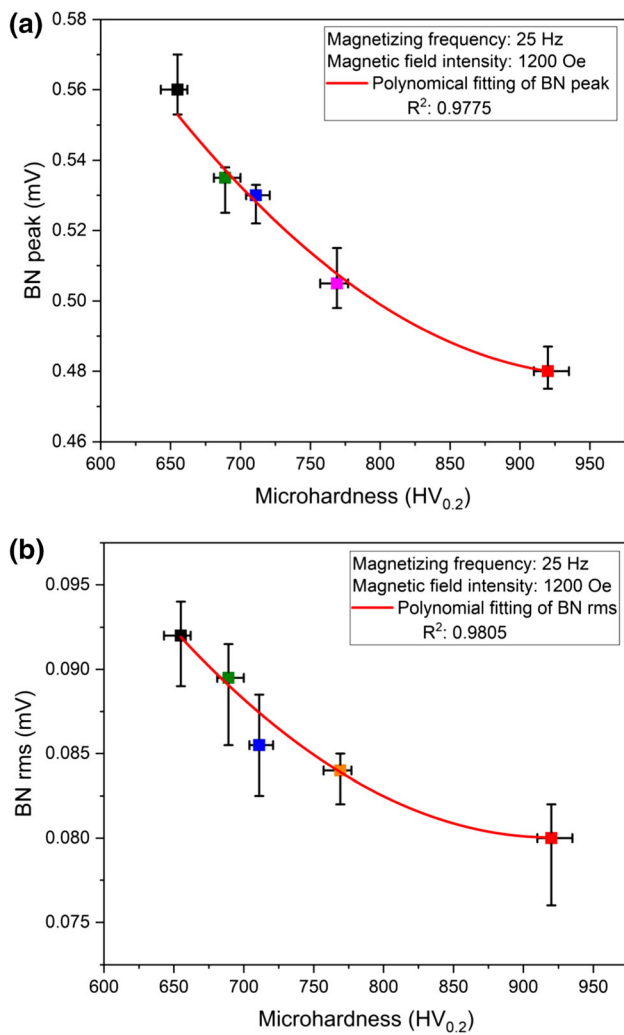


Fig. 11 Correction of microhardness with BN outcomes: **a** peak, **b** BN rms

during grinding of F1, F2 and D1 samples, which below the austenitizing temperature of 727 °C.

Barkhausen Noise Analysis

Thermal damage analysis of ground sample was carried out at different magnetic field intensities and magnetizing frequencies. BN response of ground sample was collected at various magnetizing frequency in the range of 10–40 Hz at a constant magnetic field intensity of 1000 Oe. Besides, BN responses were analysed at various magnetic field intensity in the range 300–1200 Oe at a constant 25 Hz magnetizing frequency. Generally, the depth of penetration of a magnetic field in the ground sample can be evaluated by the skin effect of the eddy current. Skin effect is a phenomenon of AC current, which is distributed within the work sample in such a way that higher AC current near the nascent surface and decreases along the depth of subsurface [35]. Skin depth increases with the decrease in

magnetic frequency and increase in magnetic field intensity [36]. Furthermore, skin depth can be adjust with high-pass and low-pass frequency filter for characterization of work material. In the present work, high–low-pass frequency filter range (10–300 kHz) was maintained for measurement of skin depth of ground surface up to 200 μm depth. The BN response from thermally damaged ground surface was measured in terms of root mean square (rms) and peak value. Figure 10a shows that magnetizing parameters has significant contribution to the BN responses. At constant magnetizing frequency, an increase in BN responses (peak and rms) was evidenced by increasing magnetic field intensity under all grinding conditions due to high penetration depth. This resulted in more number of domain wall taking part in the magnetizing process. At higher magnetic field intensity, more number of already pinned domain wall get released from the pinning sites, thus enhancing the BN responses. Lasaosa et al. [37] reported that BN responses such as rms and peak height increased with increase in magnetic field intensity. The reason is that high depth of magnetizing penetration in the ground surface. When constant magnetic field intensity was applied on the work material, an increase in magnetizing frequency leads to the increase in number of pulses per unit time, which therefore enhanced the effect of overlapping and thus raised the maximum amplitude of the power spectrum. Figure 10b shows that an increase in magnetizing frequency increases the magnitude of the rms and peak. Contrary to the above, at a lower magnetizing frequency, the BN signal was affected by the spurious noise, thus decreasing the BN signal magnitude. According to Khan et al. [38], the rms increases with the increase in the magnetic frequency and magnetic field intensity owing to the generation of more voltage pulse. It was mainly due to the mechanical characteristics of the finer grains. They reported that the poor BN response was found at higher hardness of work material. Gupta et al. [39] studied the effect of magnetizing frequencies on BN signal during surface characterization of ferritic SS409L plate after gas metal arc welding.

Figure 11 depicts the correlation between microhardness and BN signals such as peak and rms value. Figure 11a, b shows that BN responses were found to decrease with increasing thermal exposure to ground surfaces, which may be attributed to the increasing microhardness of the ground surface and subsurface. It is important to mention that microhardness also significantly contributes to the BN signal generation, as higher microhardness restricts the motion of the domain wall, which suppress the BN signal. If the presence of higher microhardness of ground sample, this decreases the mobility 180° magnetic domain and hence favours the less Barkhausen jumps. Thus, D2 specimen with higher thermal damage shows poor BN outcomes like lower peak and rms value with 0.475 mV and

0.080 mV, respectively. Besides, higher BN signals, i.e. rms of 0.092 mV and peak of 0.562 mV, were observed under base sample because of the absence of the phase transformation. Figure 11 shows the BN signal varies polynomially with microhardness and its correlation coefficient of ~ 0.9775 for peak and ~ 0.9805 for rms, respectively. The result agreed with Neslusan et al. [40], when they evaluated heat-affected zone during grinding of case hardened steel using BN technique. They found a polynomial relation between mechanical properties of the ground surface and rms.

Conclusions

The main conclusions of the present work may be summarized as follows:

1. Several side flows along with redeposition material were observed over ground surface under dry grinding.
2. Maximum thermal damage in terms of drastic microstructural change and higher microhardness was observed in the case of dry grinding due to severe plastic deformation at elevated temperature.
3. The BN response parameters, i.e. rms and peak, increased with an increase in magnetic field intensity and magnetizing frequency owing to generation of high-voltage pulse.
4. Tempered martensite formation near nascent ground surface upon grinding leads to poor BN signals, i.e. lower rms and peak value.
5. BN outcomes were polynomially correlated with the microhardness of the thermal damaged ground surface.

Acknowledgements This research work is financially supported by IIT (BHU) under sprouting grant (letter no. IIT (BHU)/Dec/2013-14/5110/L) and Institute Research Project (IIT(BHU)/R & D)/IRP/2015-16/2832). It is gratefully acknowledged.

References

1. K. Mondal, S. Das, An investigation on machinability during turning hardened steel in dry condition. *J. Inst. Eng. (India) Series C*. **99**(6), 637–644 (2018). <https://doi.org/10.1007/s40032-017-0370-1>
2. A. Shokrani, V. Dhokia, S.T. Newman, Environmentally conscious machining of difficult-to-machine materials with regard to cutting fluids. *Int. J. Mach. Tools Manuf* **57**, 83–101 (2012)
3. P. Sethuramalingam, B.K. Vinayagam, Multi objective optimization of multi wall carbon nanotube based nanogrinding wheel using grey relational and regression analysis. *J. Inst. Eng. (India) Series C* **97**(3), 407–416 (2016). <https://doi.org/10.1007/s40032-016-0238-9>
4. M. Soković, K. Mijanović, Ecological aspects of the cutting fluids and its influence on quantifiable parameters of the cutting processes. *J. Mater. Process. Technol.* **109**(1–2), 181–189 (2001)
5. M.K. Sinha, D. Setti, S. Ghosh, P.V. Rao, An investigation on surface burn during grinding of Inconel 718. *J. Manuf. Processes* **21**, 124–133 (2016)
6. A. Awale, A. Srivastava, M. Vashista, M.Z. Khan Yusufzai, Surface integrity characterization of ground hardened H13 hot die steel using different lubrication environments. *Mater. Res. Expr.* **6**(2), 026508 (2018)
7. E. Brinksmeier, E. Schneider, W. Theiner, H. Tönshoff, Non-destructive testing for evaluating surface integrity. *CIRP Ann.* **33**(2), 489–509 (1984)
8. A. Kawai, S. Iida, N. Kasai, Barkhausen noise measurement system using a three-pole probe. *J. Nondestr. Eval.* **37**(4), 80 (2018)
9. D. Moia, I. Thomazella, P. Aguiar, E. Bianchi, C. Martins, M. Marchi, Tool condition monitoring of aluminum oxide grinding wheel in dressing operation using acoustic emission and neural networks. *J. Braz. Soc. Mech. Sci. Eng.* **37**(2), 627–640 (2015)
10. M. Hadad, A. Sharbati, Analysis of the effects of dressing and wheel topography on grinding process under different coolant-lubricant conditions. *Int. J. Adv. Manuf. Technol.* **90**(9), 3727–3738 (2017)
11. G. Manimaran, R. Venkatasamy, Influence of cryogenic cooling on surface grinding of stainless steel 316. *Cryogenics* **59**, 76–83 (2014)
12. T. Tawakoli, M. Hadad, M.H. Sadeghi, A. Daneshi, B. Sadeghi, Minimum quantity lubrication in grinding: effects of abrasive and coolant-lubricant types. *J. Clean. Prod.* **19**(17–18), 2088–2099 (2011)
13. B. Nahak, A. Srivastava, M.Z. Khan Yusufzai, M. Vashista, Surface integrity assessment upon electric discharge machining of die steel using non-destructive magnetic barkhausen noise technique. *Trans. Indian Inst. Met.* **73**(4), 967–974 (2020)
14. D.C. Jiles, Dynamics of domain magnetization and the Barkhausen effect. *Czech J. Phys.* **50**(8), 893–924 (2000)
15. A. Srivastava, A. Awale, M. Vashista, M.Z. Khan Yusufzai, Monitoring of thermal damages upon grinding of hard-ened steel using Barkhausen noise analysis. *J. Mech. Sci. Technol.* **34**(5), 2145–2151 (2020)
16. W.B. Rowe, *Principles of Modern Grinding Technology* (William Andrew, Amsterdam, 2013)
17. H. Singh, V.S. Sharma, M. Dogra, Exploration of graphene assisted vegetable oil based minimum quantity lubrication for surface grinding of Ti-6AL-4V-ELI. *Tribol. Int.* **144**, 106113 (2020)
18. A.S. Awale, M. Vashista, M.Z. Khan Yusufzai, Application of eco-friendly lubricants in sustainable grinding of die steel. *Mater. Manuf. Processes* **36**(6), 702–712 (2021)
19. A. Chaudhari, A.S. Awale, A.K. Chakrabarti, Surface integrity characterization of austenitic, martensitic and ferritic stainless steel under different grinding process. *Mater. Res. Expr.* **6**(11), 1165c1169 (2019). <https://doi.org/10.1088/2053-1591/ab4f22>
20. M. Neslušán, P. Minárik, J. Grenčík, K. Trojan, K. Zgútová, Non-destructive evaluation of the railway wheel surface damage after long-term operation via Barkhausen noise technique. *Wear* **420**, 195–206 (2019)
21. S.S. Singh, A.S. Awale, A. Chaudhari, B. Nahak, Monitoring the microstructural changes of heat treated medium carbon steel by Barkhausen noise and hysteresis loop techniques. *Mater. Today: Proc.* **26**, 1198–1202 (2020)
22. A. Sorsa, S. Santa-aho, C. Aylott, B.A. Shaw, M. Vippola, K. Leiviskä, Case depth prediction of nitrided samples with Barkhausen noise measurement. *Metals* **9**(3), 325 (2019)
23. B. Guo, Q. Zhao, Wheel normal grinding of hard and brittle materials. *Int. J. Adv. Manuf. Technol.* **79**(5–8), 873–880 (2015)
24. C. Thiagarajan, R. Sivaramakrishnan, S. Somasundaram, Experimental evaluation of grinding forces and surface finish in

- cylindrical grinding of Al/SiC metal matrix composites. *Proc Inst Mech Eng Part B* **225**(9), 1606–1614 (2011)
25. W.B. Rowe, Thermal analysis of high efficiency deep grinding. *Int. J. Mach. Tools Manuf.* **41**(1), 1–19 (2001)
 26. Z. Kan, L. Wenhe, S. Lianjun, M. Heng, Investigation on grinding temperature in ultrasonic vibration-assisted grinding of zirconia ceramics. *Mach. Sci. Technol.* **23**(4), 612–628 (2019)
 27. M. Hadad, T. Tawakoli, M. Sadeghi, B. Sadeghi, Temperature and energy partition in minimum quantity lubrication-MQL grinding process. *Int. J. Mach. Tools Manuf.* **54**, 10–17 (2012)
 28. R. Irani, R. Bauer, A. Warkentin, A review of cutting fluid application in the grinding process. *Int. J. Mach. Tools Manuf.* **45**(15), 1696–1705 (2005)
 29. M. Paknejad, A. Abdullah, B. Azarhoushang, Effects of high power ultrasonic vibration on temperature distribution of workpiece in dry creep feed up grinding. *Ultrason. Sonochem.* **39**, 392–402 (2017)
 30. M.K. Sinha, R. Madarkar, S. Ghosh, P.V. Rao, Application of eco-friendly nanofluids during grinding of Inconel 718 through small quantity lubrication. *J. Clean. Prod.* **141**, 1359–1375 (2017)
 31. M. Al Bashir, M. Mia, N.R. Dhar, Investigations on surface milling of hardened AISI 4140 steel with pulse jet MQL applicator. *J. Inst. Eng. (India) Series C* **99**(3), 301–314 (2018)
 32. A. Awale, A. Srivastava, M. Vashista, M.Z. Khan Yusufzai, Influence of minimum quantity lubrication on surface integrity of ground hardened H13 hot die steel. *Int. J. Adv. Manuf. Technol.* **100**(1–4), 983–997 (2019)
 33. S. Paul, A.K. Singh, A. Ghosh, Grinding of Ti-6Al-4V under small quantity cooling lubrication environment using alumina and MWCNT nanofluids. *Mater. Manuf. Processes* **32**(6), 608–615 (2017)
 34. M. Shaw, A. Vyas, Heat-affected zones in grinding steel. *CIRP Ann.* **43**(1), 279–282 (1994)
 35. M. Vashista, V. Moorthy, On the shape of the magnetic Barkhausen noise profile for better revelation of the effect of microstructures on the magnetisation process in ferritic steels. *J. Magn. Magn. Mater.* **393**, 584–592 (2015)
 36. V. Moorthy, B. Shaw, J. Evans, Evaluation of tempering induced changes in the hardness profile of case-carburised EN36 steel using magnetic Barkhausen noise analysis. *NDT E Int.* **36**(1), 43–49 (2003)
 37. A. Lasaosa, K. Gurruchaga, F. Arizti, A. Martinez-De-Guerenu, Induction hardened layer characterization and grinding burn detection by magnetic Barkhausen noise analysis. *J. Nondestr. Eval.* **36**(2), 27 (2017)
 38. M.Z. Khan Yusufzai, A.R. Raja, S.K. Gupta, M. Vashista, Barkhausen noise analysis of friction stir processed steel plate. *Indian J. Eng. Mater. Sci. (IJEMS)* **27**(3), 670–676 (2021)
 39. S.K. Gupta, A.R. Raja, M. Vashista, M.Z. Khan Yusufzai, Effect of Gas metal arc welding on magnetic response of ferritic stainless steel. *Arab. J. Sci. Eng.* **45**(2), 1293–1303 (2020)
 40. M. Neslušán, J. Čížek, K. Kolařík, P. Minárik, M. Čilliková, O. Melikhova, Monitoring of grinding burn via Barkhausen noise emission in case-hardened steel in large-bearing production. *J. Mater. Process. Technol.* **240**, 104–117 (2017)

Publisher's Note Springer Nature remains neutral with regard to jurisdictional claims in published maps and institutional affiliations.